CALCULATION OF THE MOTION IN THE NEAR FIELD OF AN EXPLOSION IN A SOLID MEDIUM

V. P. Koryavov and G. G. Vilenskaya

Zhurnal Prikladnoi Mekhaniki i Tekhnicheskoi Fiziki, Vol. 9, No. 6, pp. 76–85, 1968

Some results are presented of calculations of motions in the near field of an explosion in a solid body for which a previously obtained equation of state is employed. The corresponding theoretical and experimental results are compared.

1. The near field of an explosion is a provisionary term. This term is conventionally applied to the high-pressure zone in which the principal energy losses of an explosion occur. For a kiloton ($4.18 \cdot 10^{19}$ erg) explosion, the near field extends over several tens of meters [1]. We know that at large pressures, the influence of shearing stresses is small, and a solid medium can be treated in the first approximation as a fluid which obeys the Pascal law. However, the equation of state of such a fluid must reflect the characteristics of a body whose pressure is associated both with a distortion of the lattice—i. e., with a change in the interatomic distance—and with atomic vibrations with respect to the equilibrium position during heating of the material.

The lack of satisfactory theoretical and experimental methods of obtaining the equations of state of a solid over a large range of parameters is associated with the substantial difficulties involved in experimenting at high pressures and high temperatures, which usually can be generated only for short periods of time. A major advance in the study of the equations of state of solid bodies was the utilization of the shock wave method. The possibility of obtaining shock adiabats for numerous materials at high pressures (up to $9 \cdot 10^6$ atm) made it possible to develop and improve methods of deriving the equations of state of solid bodies. A detailed description of these methods and the results obtained are contained in the review [2], the book [3], and in the translation [4].

A simple approximate derivation of the functions contained in the Mie-Grüneisen equation has been carried out in [5] on the basis of an analysis of known shock adiabats. Naturally, it was assumed that this equation is valid for a solid body. Shock adiabats were described by the unique equation

$$D = 1 + su \tag{1.1}$$

where D and u are the shock wave velocity and the particle velocity behind the shock, respectively, as referred to $D_0 = 1/(\rho_0 \chi)^{1/2}$, where the compressibility $\chi = -1/V(\partial V/\partial p)_S$, and the constant s was assumed equal to 1.5. From relation (1.1) and the laws of mass and momentum conservation behind the shock wave front, we obtain

$$\Delta P_{in} = \frac{\sigma(\sigma-1)}{[s-(s-1)\sigma]^2}, \quad \Delta E_{in} = \frac{1}{2}\left[\frac{\sigma-1}{s-(s-1)\sigma}\right]^2\left(1+\frac{2p_0}{\Delta p_{in}}\right) \tag{1.2}$$

Here, $\sigma = \rho/\rho_0$ is the density ratio behind and in front of the shock front; the pressure is referred to the modulus of hydrostatic pressure $K = \rho_0 D_0^2$; the energy per unit mass is referred to D_0^2; and Δ indicates that the increments of the quantities in front of the shock front are taken into account. For strong shock waves, the quantities in front of the shock wave can be safely neglected. Table 1 shows the values of these functions without allowance for back pressure and initial energy.

Table 1

σ	p_{in}	E_{in}	p_c	E_c	f_1	f_2	γ
1.0	0	0	0	0	1.0000	2.4200	1.50
1.1	0.12	0.0055	0.121	0.005	1.1671	2.1727	1.49
1.2	0.29	0.0248	0.288	0.020	1.3534	1.9673	1.47
1.3	0.54	0.0623	0.507	0.045	1.5616	1.7917	1.46
1.4	0.87	0.125	0.785	0.080	1.7949	1.6391	1.44
1.5	1.33	0.222	1.125	0.125	2.0571	1.5049	1.43
1.6	1.96	0.368	1.535	0.180	2.3529	1.3848	1.41
1.7	2.82	0.580	2.023	0.245	2.6877	1.2764	1.39
1.8	4.00	0.888	2.600	0.320	3.0682	1.1774	1.37
1.9	5.65	1.340	3.250	0.405	3.5023	1.0858	1.35
2.0	8.00	2.000	4.000	0.500	4.0000	1.0000	1.33

The Mie-Grüneisen equation has the form

$$\frac{p-p_c}{E-E_c}=\gamma\sigma \qquad \left(p_c=\sigma^2\frac{dE_c}{d\sigma}\right) \tag{1.3}$$

where γ is the Grüneisen coefficient, and p_c and E_c are the so-called cold components of the pressure and energy, respectively, which depend only on σ. Using the relations at the shock front, we obtain an equation for determining E_c:

$$\frac{dE_c}{d\sigma}-\frac{\gamma}{\sigma}E_c=\frac{p_{in}}{\sigma^2}-\frac{\gamma}{\sigma}E_{in} \tag{1.4}$$

For constant γ the solution can be written in integral form, which lends itself readily to evaluation for s = 1.5 and γ = 1 or γ = 2. For constant γ, however, the function E_c possesses a singularity at the point of limiting dynamic pressure $\sigma_* = s/(s-1)$.

In [5] it was established that for s = 1.5 and γ = 1.5 (the true Grüneisen coefficient γ approaches this value in the region where its influence on E_c is appreciable, as is the influence of E_c itself as compared to E), the terms δ^3 and δ^4 vanish in the expansion of E_c in $\delta = \sigma - 1$. Therefore, correct to terms of order δ^5, we have

$$E_c = {}^1/_2\,\delta^2 = {}^1/_2\,(\sigma-1)^2 \tag{1.5}$$

Then, for p_c we obtain

$$p_c = \sigma^2(\sigma-1). \tag{1.6}$$

Assuming that these expressions for p_c and E_c are exact for any σ, from the Mie-Grüneisen equation we obtain for γ that

$$\gamma = 2\,\frac{4-\sigma}{5-\sigma}. \tag{1.7}$$

The values of functions (1.5)–(1.7) are given in Table 1.

Figures 1 and 2 give a comparison between (1.5)–(1.7) and the relations obtained for the same functions in other papers. Curves (1) and (2) in Fig. 1 correspond to relations (1.6) and (1.5). Points 1, 2, 3, and 4 in Figs. 1 and 2 correspond to the results obtained in [6–9].

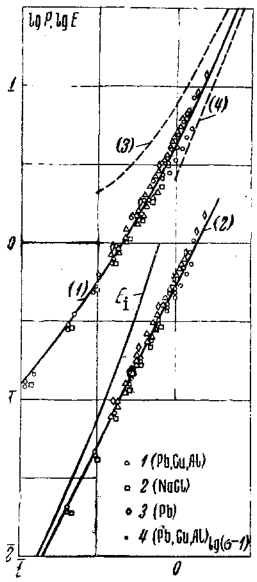

Fig. 1

In addition to the theoretical results, Fig. 2 shows experimental points 5 obtained in [10]. It can be seen that the relations adopted in the present paper (solid curves) constitute, in a certain sense, an averaging of the available curves. The logarithmic scale used in Fig. 1 reveals distinctly that the shape of the plots of p_c and E_c vs. $\sigma - 1$ is the same for different materials. The relation adopted here for p_c also correlates well with analytical results obtained after Thomas-Fermi with quantum and exchange corrections [11] (curves 3 and 4 in Fig. 1). Figure 2 shows the same relations obtained by means of (1.6) in the formulas proposed by Landau-Slater ($\gamma = \gamma_1$), Dugdale-MacDonald ($\gamma = \gamma_2$), and Zubareva-Vashchenko ($\gamma = \gamma_3$):

$$\gamma_1 = \frac{12\sigma - 5}{3(3\sigma - 2)}, \quad \gamma_2 = \frac{2}{3}\frac{(14\sigma - 5)}{(7\sigma - 4)}, \quad \gamma_3 = \frac{5}{3}\frac{(4\sigma - 1)}{(5\sigma - 2)} \tag{1.8}$$

(denoted by (1), (2), (3), respectively, in Fig. 2). It can be seen that, for mean compressions, all curves in Fig. 2 converge toward relation (1.7).

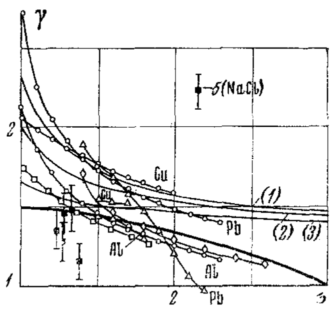

Fig. 2

The approximate equation of state obtained is suitable for constructing any relations required.

For the adiabatic curve, we obtain

$$E_s = E_c + C_1 \exp\left(-\int \frac{\gamma}{\sigma} d\sigma\right) = E_c + C_1\sigma^2 \left(\frac{5 - \sigma}{\sigma}\right)^{0.4} \tag{1.9}$$

where C_1 is the entropy function.

For the speed of sound referred to D_0, we get the following expression:

$$C^2 = f_1(\sigma) + pf_2(\sigma)$$

$$f_1(\sigma) = \frac{12\sigma}{(4-\sigma)(5-\sigma)}, \quad f_2(\sigma) = \frac{1}{\sigma}\left[3 - \frac{8-\sigma}{(4-\sigma)(5-\sigma)}\right]. \tag{1.10}$$

The value of these functions are given in Table 1.

For further analysis, it is necessary to obtain relations for the rarefaction region $\sigma < 1$. Here too, the current lack of sufficiently complete data on phase transitions and various phase states, heats of evaporation and fusion, and their variation, makes it necessary to resort to an approximate analysis. One of the possible variants is interpolation of E_c to the sublimation energy E_* (also referred to D_0^2),

$$E_c = {}^1/_2\,(\sigma - 1)^2 + (E_* - {}^1/_2)(\sigma - 1)^4. \tag{1.11}$$

For small tensions, this function has naturally the same form as for compression. The power of the second term may prove to be different (a higher power, for example). Another possibility is to neglect altogether the cold components of energy and pressure for $\sigma < 1$. Since the use of one or another approximation has little influence on results of calculations, particularly on the motion near the shock front and, at the same time, by neglecting the cold components, i.e., transition to a gas, one eliminates certain physically unacceptable situations that could arise in the computations due to bumpiness, the computations of the motion in the near field of an explosion were performed essentially with the aid of the second variant. For γ in the region $\sigma < 1$, it is also possible to obtain an interpolation formula which, for $\sigma = 1$, will satisfy the continuities of γ and its derivative, $d\gamma/d\sigma$, (in order to prevent a change in the slope of the adiabat, i.e., to provide a continuous speed of sound), and which for $\sigma \to 0$ will satisfy transition to an ideal gas ($\gamma = 2/3$). Such a relationship is provided by the formula

$$\gamma = 2\frac{4-\sigma}{5-\sigma} - \frac{14}{15}(\sigma - 1)^2. \tag{1.12}$$

2. The equation of state obtained was used to calculate the motion in the near field of an explosion. Here, the explosion source must be also modeled in some way (inner boundary condition). The basic variant of the source model

is almost standard when analyzing strong explosions in a solid medium, where high temperatures and high acoustic velocities lead to rapid compensation of the explosion-products parameters. This model is as follows: in a cavity of given radius r_{w0} in a solid medium, there occurs an instantaneous release of energy which is converted into the intrinsic energy of the material contained in the cavity. It is assumed that during the development of the explosion, all the parameters of the material contained in the cavity—of the explosion products—are distributed uniformly along the radius of the cavity and that expansion is adiabatic. It is further assumed that the products are an ideal gas with a constant specific heat ratio $\varkappa$. Then, for the pressure at the wall, we have

$$p_w = p_{w0}\,(r_{w0}/r_w)^{3\varkappa}. \tag{2.1}$$

Specific heat ratios of 1.47 and 1.2 were used in the computations.

The second variant of the source model, previously examined by Gubkin, was as follows. Against the wall of the initial cavity in a solid medium there impinges a freely dispersing (zero pressure) mass of material M, whose kinetic energy is equal to the explosion energy, whose particle velocity U is linear, and whose density ρ is constant along the radius. Reflection from the cavity wall generates a pressure P_W (the use of a capital P denotes dimensional pressure), while a shock wave propagates from the wall in the dispersing material. Since reflection is accompanied by strong compression, while the shock wave is deflected by the oncoming flow of material, it may be roughly assumed that the wave does not separate from the wall and that the parameters behind the wave are constant. Then the pressure at the wall is

$$P_w = \frac{3MU^2_{\varkappa}}{4\pi r^3_{w0}}\left(\frac{t_0}{t}\right)^5, \tag{2.2}$$

where $t_0 = r_{w0}/U_{in}$ is the arrival time of the dispersion boundary at the point r_{w0}, and U_{in} is the mass velocity at the dispersion boundary, which is related to the energy and mass by the following expression:

$$U_{in}^2 = {}^{10}/_3\,E/M \tag{2.3}$$

Thus, at time t_0 we have

$$P_{w0} = \frac{2.5}{\pi}\frac{E}{r^3_{w0}}, \quad \left(\frac{dP_w}{dt}\right)_0 = -\frac{5P_{w0}}{t_0}. \tag{2.4}$$

In the calculation of the motion in the near field, the pressure was given in the form of an exponential relation with respect to time plus a function that described the change in pressure caused by an increase in the cavity radius, of the same type as in the first version of the source

$$P_w = P_t e^{-kt} + P_r\,(r_{w0}/r_w)^{3\varkappa}. \tag{2.5}$$

Here, t has its zero at the instant of arrival of the dispersion boundary at the cavity wall (from t_0)

$$P_r = \frac{3(\varkappa-1)E}{4\pi r^3_{w0}}, \quad P_t = \frac{(13-3\varkappa)E}{4\pi r^3_{w0}}, \quad k = \frac{50}{(13-3\varkappa)t_0}. \tag{2.6}$$

The equations of motion in the near field of an explosion, in Lagrange variables, have the form

$$U = \frac{\partial r}{\partial t}, \quad \frac{\partial U}{\partial t} = -r^2\frac{\partial P}{\partial m},$$

$$\frac{\partial\rho}{\partial t} = -\rho^2\frac{\partial(r^2U)}{\partial m}, \quad \frac{\partial e}{\partial t} = -P\frac{\partial V}{\partial t}, \tag{2.7}$$

where U is the mass velocity, P is pressure, ρ is density, $V = 1/\rho$, e is the intrinsic energy per unit mass, r is an Euler coordinate, t is time, and m is the mass per unit solid angle. To these equations one must add the equation of state discussed in section 1, together with the boundary conditions. The condition at the inner boundary (the source model) has been examined above. The conditions at the shock wave constitute conventional mass and momentum conservation conditions which in the case of (1.1) lead to (1.2).

Numerical calculations were performed on the basis of a difference analog in two space variables with a substituted shock wave front. The latter means that the front represents a discontinuity with known relationships between the quantities in front of and behind the front. The mass velocity at the front is determined by extrapolation.

Below, we present some computational formulas for one of the variants. Here, n is the number of a layer in time and i is the number of a point in space.

Calculation of internal points:

$$u_i^{n+1} = u_i^n - \Delta t \left[(r_i^n)^2 \frac{p_{i+1}^n - p_{i-1}^n}{m_{i+1}^n - m_{i-1}^n} \right],$$

$$r_i^{n+1} = r_i^n + u_i^{n+1} \Delta t;$$

$$V_i^{n+1} = V_i^n + \Delta t \frac{(r_{i+1}^n)^2 u_{i+1}^{n+1} - (r_{i-1}^n)^2 u_{i-1}^{n+1}}{m_{i+1}^{n+1} - m_{i-1}^{n+1}},$$

$$e_i^{n+1} = (E_c)_i^{n+1} + \frac{e_i^n - (E_x)_i^n}{1 + (\gamma_i^n / V_i^n)(V_i^{n+1} - V_i^n)};$$

the pressure p is calculated from the equation of state.

Calculation at the cavity wall:

$$u_0^{n+1} = u_0^n - \Delta t \left(\frac{r_0^n + r_1^n}{2} \right)^2 \left(\frac{p_1^n - p_0^n}{m_1 - m_0} \right),$$

$$r_0^{n+1} = r_0^n + u_0^{n+1} \Delta t, \quad p_0^{n+1} = p_{w0} (r_{w0} / r_0^{n+1})^{3\varkappa},$$

$$V_0^{n+1} = V_0^n + \Delta t \frac{(r_1^n)^2 u_1^{n+1} - (r_0^n)^2 u_0^{n+1}}{m_1 - m_0};$$

the energy e is calculated from the equation of state.

Calculation of the shock wave front:

$$r_f^{n+1} = r_f^n + \Delta t D_f^n, \quad m_f^{n+1} = {}^1/_3 \rho_0 (r_f^{n+1})^3,$$

$$u_f^{n+1} = u^{n+1} \left[1 - \frac{(u_f^n - u^n)\, m_f^n}{u_f^n m_f^{n+1}} \right]^{-1},$$

Here,

$$u = u_{k-1} + \left(\frac{m_f - m_k}{m_k - m_{k-1}} \right) (u_k - u_{k-1})$$

(k is the number of the internal point closest to the front)

$$D_f^{n+1} = D_0 + s u_f^{n+1}, \quad p_f^{n+1} = \rho_0 u_f^{n+1} D_f^{n+1},$$

$$e_f^{n+1} = {}^1/_2 (u_f^{n+1})^2, \quad V_f^{n+1} = 1 / \rho_0 (1 - u_f^{n+1} / D_f^{n+1}).$$

Table 2 and Figs. 3–9 show the results of computations for the first variant of the explosion source, with the initial pressure at the cavity wall referred to $K = \rho_0 D_0^2$, $p_{w0} = 11.88$, a reduced initial radius $R_{w0} = 1$ m/kton$^{1/3}$, and $\varkappa = 1.47$. In Table 2 t, R_w, and R_f are the time, in milliseconds, and the radii of the cavity and the front, in meters, respectively, referred to the cube root of the explosion energy q, in kilotons (i.e., $t = t_p/q^{1/3}$, $R_w = r_w/q^{1/3}$, $R_f = r_f/q^{1/3}$, where t_p is dimensional time); u_f is the dimensionless mass velocity behind the front (velocity referred to D_0); $\sigma_f = \rho_f/\rho_0$, p_f is the dimensionless pressure at the front (pressure referred to K); E_w is the residual energy in the products in the cavity; and E_k is the total kinetic energy of motion of the medium, as a percent of the total explosion energy. It is obvious that the residual energy of the explosion was converted to the intrinsic energy of the medium. The intrinsic-energy integral was also evaluated in the computations, while the conservation of total energy was used to check the accuracy of the solution. In Figs. 3 and 4, the dimensionless pressures and the dimensionless mass velocity at the front (solid curves) are plotted in logarithmic scale vs. the reduced radius of the front.

The general nature of the time-variation of pressure, velocity, density, and intrinsic-energy profiles is shown in Fig. 5. Figures 6–8 show the pressure, velocity, and density (more precisely $\sigma - 1$) profiles referred to their values at the front, along a radius referred to the radius of the front, for various times. Figure 9 shows, in reduced coordinates, the variation in time of the cavity radius and the radius of the shock wave front.

In order to determine the influence of explosion energy concentration on the motion in the near field, we calculated variants in which the concentration was magnified eight times (curves denoted by 1 in Figs. 3, 4, and 9) and was diminished eight times (curves denoted by 2). It may be seen that a difference in the concentration affects the shock wave parameters only in the proximity of the explosion cavity.

Figures 3 and 4 show the motion computed on the basis of the second variant of the explosion source—with a pressure peak—(dashed curve denoted by 3). A discrepancy with the results obtained by the first variant is to be observed only in direct proximity of the cavity. The profiles of the motion parameters also tend rapidly (with an increase of the shock front radius by 10%) toward the profiles obtained by the first variant.

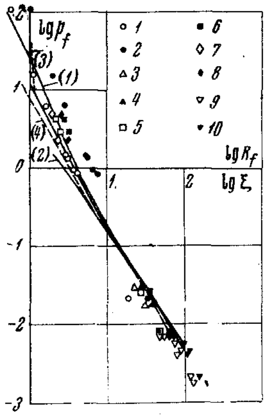

Fig. 3

Computation of variants with $\varkappa$ = 1.2 revealed a small influence of $\varkappa$ on the attenuation of the pressure and velocity at the front. The results obtained for this value of $\varkappa$ by the basic variant are shown by the dashed curve denoted by 4 in Figs. 3 and 4.

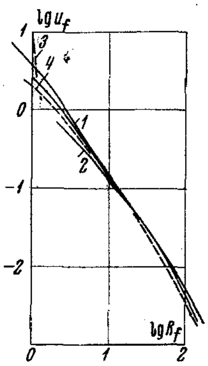

Fig. 4

3. Only individual results of computations of motions in the near field of strong explosions in solid media have been published to date [1, 12–14]. Figure 10 shows the results of shock-wave compression for several rocks (1—marble [15]; 2—quartz [16]; 3—gabbro [17]; (4), (5), (6)—granite [12, 18, 19]; 7—diabase; 8—tuff [13]). On the basis of these data, it is possible to obtain the corresponding D_0 and $K = \rho_0 D_0^2$ for tuff, granite, and rock salt, with the aim of recalculating the results obtained in [1, 12–14].

Table 2

t	R_w	R_f	U_f	σ_f	p_f	E_w	E_k
0	1.0	1.0	2.5	2.11	11.88	100.0	0
0.0221	1.178	1.340	1.888	1.971	7.232	79.5	10.3
0.0796	1.510	2.016	1.204	1.751	3.377	56.0	21.4
0.245	2.074	3.383	0.626	1.477	1.215	35.8	30.0
0.653	2.808	5.801	0.300	1.261	0.436	23.3	35.1
1.48	3.660	9.742	0.147	1.137	0.180	16.0	39.0
3.07	4.693	16.40	0.0737	1.071	0.0818	11.3	41.7
6.35	6.209	29.15	0.0353	1.035	0.0371	7.6	44.6
11.65	8.718	49.17	0.0173	1.017	0.0177	4.7	51.3
21.7	12.43	86.01	0.0056	1.006	0.0056	2.8	63.2
38.9	16.09	149.24	0.0020	1.002	0.0020		

Since the various papers deal with media with somewhat differing parameters, the values used by us for comparison and in computations are listed below:

Medium	ρ_0	D_0	K	ν_1	ν_2
Tuff	2.00	1.8	65	0.562	0.274
Salt	2.24	3.0	202	0.820	0.665
Granite	2.67	2.4	154	0.748	0.486
Calculated	2.70	3.7	368	1.000	1.000

Here, ρ_0 is taken in g/cm^3, D_0 in km/sec, K in kbar; ν_1 and ν_2 will be identified below.

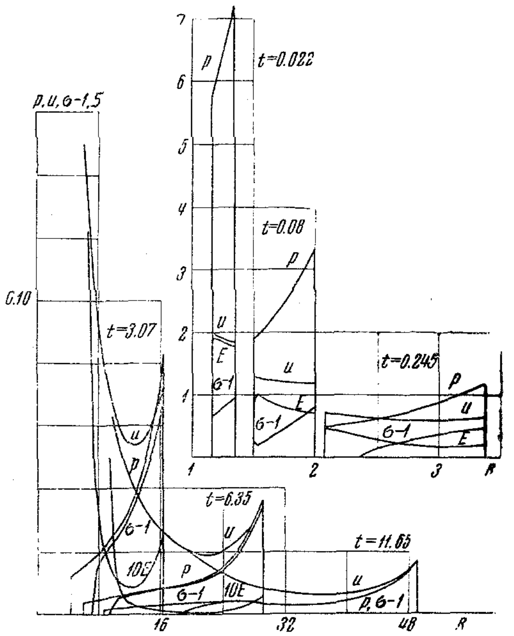

Fig. 5

We present the characteristics of explosions in various media, including the corresponding references in the literature.

Explosion	Medium	q	R_{w0}	ξ_{w0}	Designation	Reference
Rainier	tuff	1.7	0.985	0.554	1 2	[1, 13, 14]
Gnome	salt	3.1	1.32	1.08	3 4	[14]
Hardhat	granite	5.0	concentrated		5 6	[12–14]
Shoal	granite	12.5	concentrated		7 8	[12–14]
Trinitrotoluene	granite	0.01 0.001	5.32	3.98	9 10	[20]
	calculated		0.5, 1, 2;	0.5, 1, 2		

Here, q is energy of the explosion in kilotons, R_{w0} is the initial reduced radius ($R_{w0} = r_{w0}/q'^{1/3}$), and ξ_{w0} is the initial value of ξ (to be mentioned below).

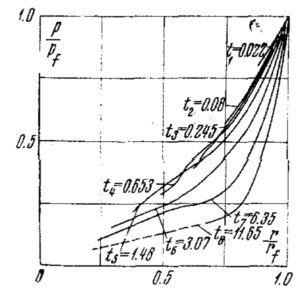

Fig. 6

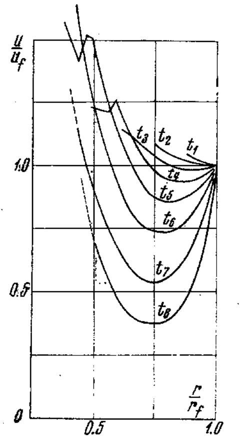

Fig. 7

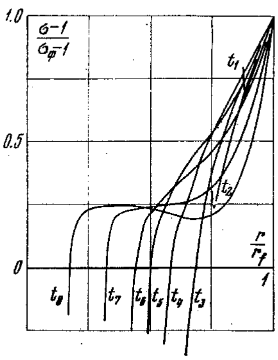

Fig. 8

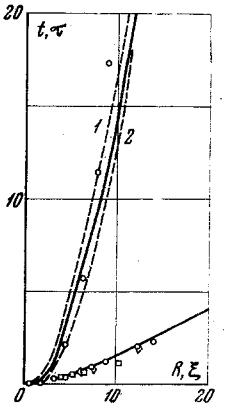

Fig. 9

Experimental data obtained for the pressure at the front P_f (in kbar) are compiled in Table 3 as a function of the radius of the front (in meters), as well as the quantities $p_f = P_f/K_f$ and $R_f = r_f/q^{1/3}$.

Table 3

r_f	P_f	R_f	p_f	lg R_f	lg p_f	ξ	lg ξ
			Hardhat, granite				
4.85	660	2.83	4.28	0.452	0.632	2.12	0.327
5.51	450	3.22	2.92	0.508	0.466	2.41	0.382
61.8	4.0	36.1	0.026	1.558	$\bar{2}.416$	27.0	1.432
109.7	1.2	64.2	0.0078	1.808	$\bar{3}.892$	48.0	1.682
			Shoal, granite				
5.79	740	2.49	4.8	0.397	0.682	1.87	0.272
7.07	350	3.05	2.24	0.484	0.35	2.28	0.359
			Gnome, salt				
40	6	27.4	0.0297	1.438	$\bar{2}.474$	22.5	1.352
55	3.5	37.65	0.0173	1.576	$\bar{2}.239$	30.9	1.490
			Rainier, tuff (theoret.)				
1.17	6850	0.98	105	$\bar{1}.994$	2.023	0.55	$\bar{1}.744$
2.3	1000	1.93	15.4	0.286	1.187	1.08	0.036
3.3	400	2.76	6.15	0.442	0.789	1.55	0.192
40	1.4	33.55	0.0216	1.526	$\bar{2}.334$	18.85	1.276
	94	5.2	1.45	0.716	0.16	2.92	0.466
	86	5.3	1.32	0.725	0.122	2.98	0.474
	60	6.6	0.92	0.820	1.966	3.7	0.569
	54	7.4	0.83	0.87	1.92	4.15	0.618
			Trinitrotoluene explosions, granite				
		65	0.0073	1.813	$\bar{3}.865$	48.6	1.687
		73	0.0075	1.864	$\bar{3}.876$	54.6	1.738
		100	0.0056	2.0	$\bar{3}.747$	74.8	1.874
		112	0.0040	2.05	$\bar{3}.602$	83.8	1.924
		120	0.0047	2.08	$\bar{3}.67$	89.8	1.954
		158	0.0021	2.198	$\bar{3}.333$	118.0	2.073
		178	0.0017	2.31	$\bar{3}.236$	133.0	2.125

The values of the front and cavity radii (in meters) are compiled in Table 4 as a function of time t_p (in milliseconds) for various explosions, together with the values of $R = r/q^{1/3}$ and $t = t_p/q^{1/3}$. Figures 3, 4, and 9 show a comparison of these data with the theoretical results. The theoretical results were also compared with the results in [21, 22].

Table 4

t_p	r	t	R	τ	ξ
		Rainier, tuff, shock wave			
0.2	4	0.17	3.35	0.046	1.88
1.68	9.54	1.41	8.00	0.336	4.50
4.2	16	3.52	13.4	0.965	7.54
5.0	19	4.19	16.0	1.15	9.0
10	30	8.4	25.2	2.3	14.2
		7.1	22	1.945	12.4
		Rainier, tuff, cavity (theoret.)			
0	1.17	0	0.935	0	0.554
8.9	10	7.46	8.4	2.045	4.72
25	13.57	21	11.45	5.75	6.44
50	16.8	42	14.2	11.5	7.98
75	18.57	63	15.7	17.3	8.83
		Hardhat, granite, shock wave			
0.86	7.34	0.50	4.29	0.246	3.21
1.22	9.48	0.71	5.55	0.346	4.15
1.64	12.36	0.96	7.22	0.467	5.4
2.15	15.02	1.26	8.79	0.614	6.57
3.77	24.14	2.2	14.1	1.07	10.55
		Shoal, granite, shock wave			
0.336	5.79	0.14	2.5	0.07	1.87
0.534	7.06	0.23	3.04	0.112	2.275
0.540	7.06	0.23	3.04	0.113	2.275
0.75	8.31	0.32	3.58	0.157	2.68
2.68	19.39	1.158	8.35	0.564	6.25
3.54	23.79	1.525	10.26	0.742	7.68
5.68	35.63	2.45	15.36	1.192	11.5

Our calculations indicate that the motion in the near field depends on the concentration of explosion energy, i.e., on the pressure within the initial cavity. If the media differ only in the modulus K, the patterns of motion are similar when the ratios of initial pressure to K are the same. For this reason, in order to compare results for various media, we introduce the variables

$$\xi = \nu_1 r / q^{1/3}, \quad \tau = \nu_2 t_p / q^{1/3}, \quad \nu_1 = (K / K_*)^{1/3}, \quad \nu_2 = \nu_1 D_0 / D_{0*} \tag{3.1}$$

where the asterisk denotes values corresponding to the reference medium.

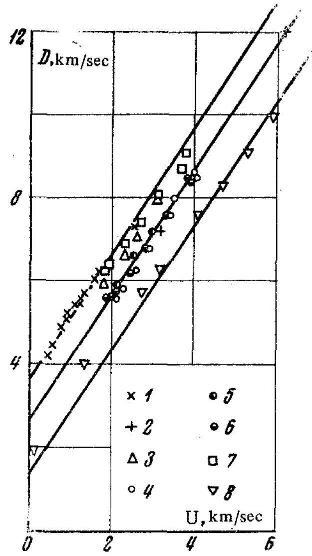

Fig. 10

From Fig. 3, it can be seen that the use of the variables (3.1) provides a much better agreement between results in the near field for various media. The conventional similarity with respect to the cube root of the explosion energy, which is the same for different media and energy concentrations, is apparently better suited for use in the far field. This may be attributable to the fact that at large distances any explosion is highly concentrated. In addition, the use of the variables (3.1) leads to a good correlation of results for shock-wave and cavity radii in various media (see Fig. 9 and Table 4).

In conclusion we note that the good agreement with experimental data is an indication for the accuracy of our description of the medium and explosion source.

REFERENCES

1. G. W. Johnson, G. H. Higgins, and K. I. Violet, "Underground nuclear explosions," collection: Underground Nuclear Explosions [Russian translation], Izd-vo inostr. lit., Moscow, p. 1, 1962.

2. L. V. Al'tshuler, "Application of shock waves in high-pressure physics," Usp. fiz. nauk, vol. 85, no. 2, p. 197, 1965.

3. Ya. B. Zel'dovich and Yu. P. Raizer, Physics of Shock Waves and High-Temperatures Hydrodynamic Phenomena [in Russian], Fizmatgiz, Moscow, 1963.

4. Dynamic Investigations of Solids at High Pressures, Mir, Moscow, 1965.

5. V. P. Koryavov, "Approximate equation of state of solid bodies," PMTF, no. 5, p. 123, 1964.

6. L. V. Al'tshuler, S. B. Kormer, A. A. Bakanova, and R. F. Trunin, "Equations of state of aluminum, copper, and lead in the high-pressure range," ZhETF, vol. 38, no. 3, p. 790, 1960.

7. L. V. Al'tshuler, L. V. Kuleshova, and M. N. Pavlovskii, "Dynamic compressibility, equations of state, and electrical conductivity of NaCl at high pressures," ZhETF, vol. 39, no. 1, (7), p. 16, 1960.

8. L. V. Al'tshuler, A. A. Bakanova, and R. F. Trunin, "Shock adiabats and zero isotherms of seven metals at high pressures," ZhETF, vol. 42, no. 1, p. 91, 1962.

9. S. B. Kormer, A. I. Funtikov, V. D. Urlin, and A. N. Kolesnikova, "Dynamic compressibility of porous metals in the equation of state with variable specific heat at high temperatures," ZhETF, vol. 42, p. 686, 1962.

10. B. Alder, "Physical experiments with strong shock waves," in: Solid Bodies Under High Pressures, [Russian translation], Mir, Moscow, p. 430, 1966.

Moscow, p. 430, 1966.

11. N. N. Kalitkin, "Model of the Thomas-Fermi atom with quantum and exchange corrections," ZhETF, vol. 38, p. 1534, 1960.

12. T. R. Butkovich, "Calculation of the shock wave from an underground nuclear explosion in granite," J. Geophys. Res., vol. 70, no. 4, p. 885, 1965.

13. F. Holzer, "Measurements and calculations of peak shock wave parameters from underground nuclear detonations," J. Geophys. Res., vol. 70, no. 4, p. 893, 1965.

14. F. Holzer, "Calculation of seismic source mechanism," Proc. Roy. Soc., vol. 29, no. 1422, p. 408, 1966.

15. A. N. Dremin and G. A. Adadurov, "Shock adiabat of marble," Dokl. AN SSSR, vol. 128, no. 2, p. 261, 1959.

16. L. V. Al'tshuler, R. F. Trunin, and G. V. Simakov, "Shock wave compression of periclase and quartz, and the composition of the lower mantle of the earth," Fizika Zemli, no. 10, 1965.

17. D. Hughes and R. McQueen, "Density of basic rocks at very high pressures," Dynamic Investigation of Solid Bodies at High Pressures [Russian translation], Mir, Moscow, 1965.

18. G. A. Adadurov, A. N. Dremin, and Yu. N. Ryabinin, "Behavior of certain materials under shock-wave compression," PMTF, no. 6, p. 115, 1964.

19. R. G. McQueen, S. P. Marsh, and J. N. Fritz, "Hugoniot equation of state of twelve rocks," J. Geophys. Res., vol. 72, no. 20, p. 4999, 1967.

20. B. D. Khristoforov and A. N. Romashov, "Determination of compression-wave parameters in rocks," Fizika goreniya i vzryva [Combustion, Explosion, and Shock Waves], no. 1, p. 137, 1967.

21. V. M. Gogolev, V. G. Myrkin, and G. Ya. Yablokova, "Shock wave calculations for explosions in solid media," Nauchn.-tekhn. problemy goreniya i vzryva [Combustion, Explosion, and Shock Waves], no. 1, p. 80, 1965.

22. N. F. Vanyagin, V. M. Gogolev, V. G. Myrkin, and A. N. Khanukaev, "Propagation of stress waves during explosions in rocks," Zap. Leningr. gorn. in-ta, vol. 44, no. 1, 1961.

21 March 1968

Moscow